Journal of Urban and Environmental Engineering, v.15, n.2, p.147-158

ISSN 1982-3932
doi: 10.4090/juee.2021.v15n2.147158

Journal of Urban and Environmental Engineering

www.journal-uee.org

ANALYSIS OF MULTIPHASE FLOW UNDER PARTIALLY OPEN FLOODGATES IN A SITUATION OF MAXIMUM FLOOD USING A NUMERICAL MODEL

Alexson Caetano da Silva[1*], José Roberto Gonçalves de Azevedo[1], Luciete Alves Bezerra[2] and Jaime Joaquim da Silva Pereira Cabral[3]

[1]*Department of Civil Engineering, Federal University of Pernambuco, Brazil*
[2]*Department of Mechanical Engineering, Federal University of Pernambuco, Brazil*
[1]*Department of Civil Engineering, University of Pernambuco, Brazil*

Received 15 July 2021; received in revised form 15 November 2021; accepted 15 December 2021

Abstract: Hydraulic gates are structures widely used to control discharge and runoff depth in irrigation channels, sewage treatment stations, dams, in the São Francisco River transposition system, among other hydraulic structures. Flaws in the mechanisms for opening the gates are recurrent in these structures. These failures in the operation of the gates combined with a critical event of maximum flood can lead to the collapse of the system. In this work, a study was carried out of a flow under a partially open hydraulic gate in a channel with the maximum amount level, using a CFD program, Ansys CFX. This software uses the Finite Volume Method for domain discretization. In order to generate the model, a mesh convergence test was carried out, the residues of the simulations in the permanent and transient states of the flow were also compared. The study identified a region of flow separation near the gate. Another point studied was the hydraulic pressure generated by the flood in the structure, with the finding of a region of elevation of the values of the stresses that coincides with the zone of separation of the flowe.

Keywords: CFD, Hydraulic Gates, Ansys CFX

[*] Correspondence to: Alexson Caetano da Silva. E-mail: alexsoncaetano@hotmail.com

INTRODUCTION

Hydraulic gates are structures widely used to control discharge and flow depth in irrigation channels, sewage treatment plants, dams and other hydraulic structures. Two of the main practical importance of hydraulic gates are their use as structures for measuring and controlling floods. Mechanical failures in the operation of these structures are recurrent and can prevent their total or partial opening.

Defects in the floodgate drive systems combined with extreme floods are a matter of concern for engineers and technicians who design and operate these structures. The São Francisco River Integration Project with Hydrographic Basins of the Northeast Northeast (PISF), which will bring water to the interior of the Northeast, used hydraulic gates in several of its structures and problems that hinder its operation has a great social impact for the population.

The advancement of computational capacity over the last few decades has provided the solution of fluid flow equations through the numerical solution of Reynolds' average equations for Navier-Stokes (RANS), enabling the use of turbulence models that have proven to be a good alternative to analyze the flow flow in a penstock.

Cassan and Belaud (2012) studied the flow upstream and downstream of a hydraulic gate both experimentally and numerically using the Reynolds mean equations for Navier-Stokes in two dimensions with the Finite Volume Method. Special attention was paid to channels with a large cross section and submerged, which is a very frequent situation in distribution channels and little addressed in the literature. The authors produced a structured 2D mesh, however in the regions below the gate, due to its strong flow acceleration, the mesh was adapted locally. The researchers concluded that the choice of the turbulence model largely interferes with the final estimate of the contraction coefficient in submerged flow channels with large opening of the gates.

Akoz *et al.* (2009) simulated and analyzed, through computational fluid dynamics, a flow below a gate with the same conditions as an experimental flow performed in the laboratory. The numerical results for the speed field and the free surface profile of eight computational meshes were compared by the authors with the experimental data. Based on the comparison, the most suitable mesh was chosen from the eight simulations. The study employed further refinement in the region close to the base of the penstock. The researchers came to the conclusion that the local density of the mesh influences the degree of accuracy of the numerical results in relation to the experimental results, for the speed field and the free surface profile.

Jesudhas *et al.* (2016), Teng & Yang (2016), Momplot *et al.* (2016), Ahmed *et al.* (2020), Ciocan *et al.* (2016), Ferdos & Dargahi (2016) (a), Ferdos & Dargahi (2016) (b), Hardy *et al.* (2005), Jesudhas *et al.* (2019), Koutrouveli *et al.* (2018), Li *et al.* (2019), Li *et al.* (2017), Lu *et al.* (2018), Maranzoni & Tomirotti (2020), Momplot *et al.* (2016), Talebpour & Liu (2018), Taylor *et al.* (2015), Yang *et al.* (2019) and Zhang *et al.* (2020), also studied hydraulic structures with the CFD.

This work investigates the multiphase flow in a completely filled channel upstream with a partially open gate, in order to represent a failure situation in the opening operation of the structure. For numerical modeling, a computational fluid dynamics program, Ansys CFX, was used. For the analysis it was considered a channel of rectangular section (34 cm of base and 49 cm of height) and a total length of 5 m. The channel has a bottom with a slope of 0.005m / m. In addition, a gate was installed in the middle of the channel with beveled edges and an opening of 15 cm, which allows a partial passage of the hydraulic flow. In order to analyze a design limit situation, the inlet flow was considered to be the channel completely filled, indicating a maximum design flood hitting the penstock structure.

The study performs a deep analysis of the meshes and through the convergence test, the one that best represents the flow is chosen. The flow within the channel was considered biphasic, composed of air and water. A comparison was also made between the data of the permanent and transient regimes, and it was found that the mean square error was lower for the transient regime. The model showed a region of recirculation close to the gate that reflects the values of the effective stresses and in the structure and that must be taken into account during the structural designs of this structure because it causes differential efforts. Still, it identified that this zone separates the flow taking part of it out of the domain and another part is pushed under the gate. The study shows that numerical tools using computational fluid dynamics are sufficiently advanced to assist in the analysis of the flow under floodgate subject to extreme situations of floods and mechanical failures that hinder the opening of the structure.

MATHEMATICAL MODELING

The equations that govern fluid dynamics and which are solved in the CFD model are: the mass conservation equation and the momentum equation. These are given respectively by:

$$\partial\rho/\partial t + \nabla \cdot \rho\mathbf{u} = 0 \quad (1)$$

$$\partial(\rho\mathbf{u})/\partial t + \nabla \cdot \rho(\mathbf{u}\mathbf{u}) = -\nabla p + \nabla \cdot \tau + F_s \quad (2)$$

The variables used in **Eq. (1)** and **(2)** are described as **u**, ρ, p, t, τ, F_S, being respectively the velocity, density, pressure, time, force tensor and surface tension contribution term. According to Versteeg & Malalasekera (2007), liquids and gases that flow at low speeds can be considered incompressible, so the flow field in CFD modeling can be obtained by solving the equations of continuity and amount of movement.

The free surface between water and air is modeled using the finite volume method, where each cell is composed of a fraction of each of the two phases (water and air). As it is a multiphase flow, with the presence of air and water, the multiphase model of finite volumes is used, so the volume fraction is defined as **Eq. (3)**:

$$\partial(\rho\alpha_q)/\partial t + \nabla\cdot(\rho\alpha_q\mathbf{u}) = 0 \quad (3)$$

The following restriction is necessary for the application of the model **Eq. (4)**:

$$\alpha_l + \alpha_g = 1 \quad (4)$$

where α_l, α_g, α_q, are the volume fractions of the liquid, gas, and liquid and gaseous phases, respectively. The method used for the numerical discretization of the equations that govern the model is the Finite Volume Method. The chosen turbulence model is the standard k-ε, developed by Launder & Spalding (1974), this is widely used and validated in free flow problems, according to Faure *et al.* (2004), Lira (2014), Sinha *et al.* (2014).

METHODOLOGY

Geometry and Mesh Generation

The modeled geometry consists of a 5 m long channel and a cross section with dimensions of 34 cm of base and 49 cm of height. The channel has a bottom with a slope of 0.005m / m. In addition, a gate was installed in the middle of the channel with chamfered edges (45º angle of the chamfer) and an opening of 15 cm, allowing the passage of water under it, simulating a failure in interrupting the opening operation of the channel. For the analyzes, a Cartesian axis was defined where the abscissa is the "x" axis (axis along the channel) with its zero below the gate and the ordered "z" axis (axis perpendicular to the bottom of the channel) with its zero at the base of the channel, as shown in **Fig. 1.**

The process of choosing the most efficient mesh for the model takes place with the mesh convergence test, where meshes are generated with varying degrees of refinement and the mesh that with the lowest computational cost best represents the phenomenon will be used to work all the results. Thus, five meshes were defined according to **Table 1**.

Fig. 1 Arrangement of coordinate axes along the channel.

Table 1. Number of nodes and elements for each mesh.

Mesh	Number of nodes	Number of elements
1	3097	7183
2	12219	33634
3	23043	69608
4	62071	218138
5	209322	824718

Physical Definitions

After modeling the mesh, the physical parameters of the model were defined. The domain resulting from the modeling can be seen in **Fig. 2**. (a) Inlet: On the inlet face (face with black arrows, as shown in **Fig. 2**), the speed of the hydraulic flow that entered normal to it was indicated. Taken as 1.50 m/s, as they are usual values for flow in channels. The entire face was filled by flow in order to model the situation of maximum flow in the hydraulic section of the channel. (b) Open: On the faces where this domain was selected (faces with blue arrows, according to **Fig. 2**), a relative pressure of 0 Pa was adopted. The faces selected with this domain were the top and the exit face. (c) Walls: For all walls (bottom and sides, and penstock faces) the No Slip wall boundary condition was applied. The roughness of the walls was considered null, this consideration is valid if the materials of the walls and backgrounds are glass or acrylic, according to Sanagiotto *et al.* (2019). The boundary layer was also modeled to define the flow close to the walls and bottom.

The multiphase model was chosen as homogeneous (Multiphase Homogeneous Model), where there is a macroscopic mixture of air and water and all fluids have the same speed fields, as well as other relevant fields, such as temperature, turbulence, pressure, etc. The surface tension coefficient at 25 ºC and 1 atm of 0.0732 N/m was considered, according to Çengel & Cimbala (2007) and the free surface model to simulate the interface between air and water.

Defining the Flow Regime

Starting from the premise of obtaining the best solution with the lowest possible computational cost, the analysis of the model in the stationary regime was first considered, considering as a stop criterion an average square error (RMS) of 0.001, as recommended by Celik *et al.* (2008). All meshes converged to this value, however when comparing the residues between the most refined mesh in the transient state and the most refined

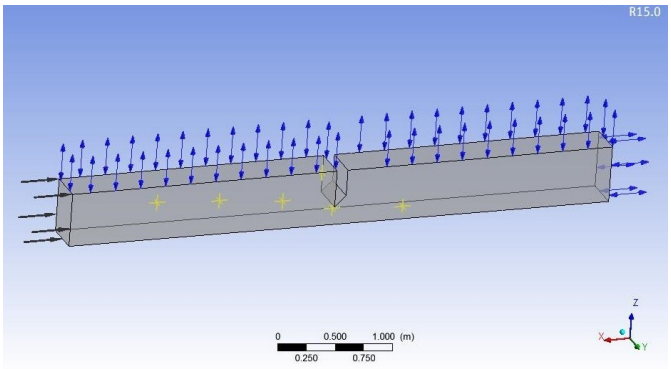

Fig. 2 Computational domain with the physical characteristics of the flow.

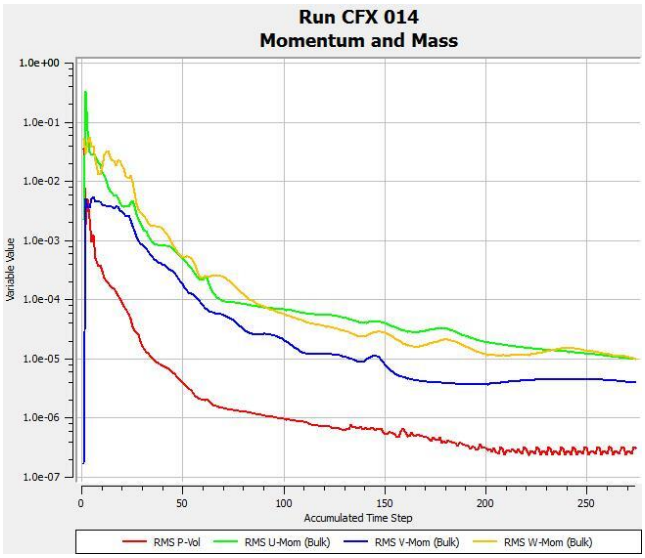

Fig. 3 RMS for the simulated models stationary regime.

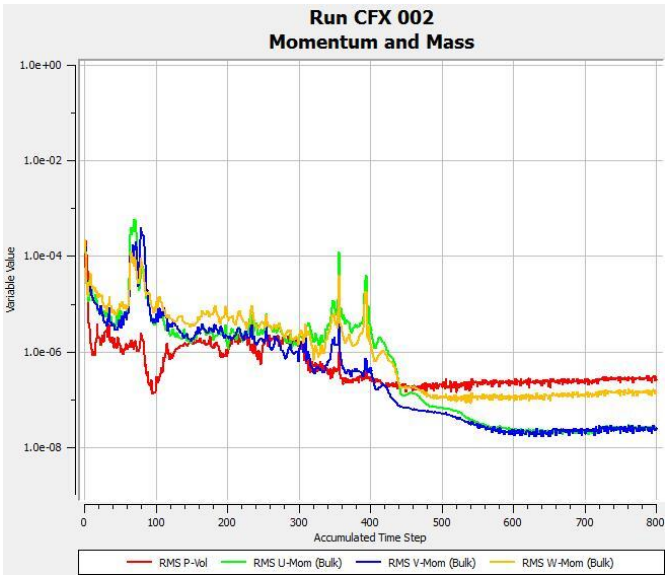

Fig. 4 RMS for the simulated models transient regime.

mesh in the steady state, there is a considerable decrease in the RMS value going from 10^{-5}, as shown in **Fig. 3**, for 10^{-7}, as shown in **Fig. 4,** indicating that the transient regime best represents this phenomenon.

Table 2. Courant number values for mesh 3.

Time step (s)	0.0125	0.025	0.10	0.20	0.40	0.80
Courant number	1.7	3.5	14.0	28.0	56.0	114.0

Table 3. x and y coordinates of the analysis points.

Point	Coordinate x	Coordinate y
1	-1.57	0.27
2	-1.02	0.26
3	-0.42	0.20
4	-0.07	0.44
5	0.04	0.09
6	0.70	0.05

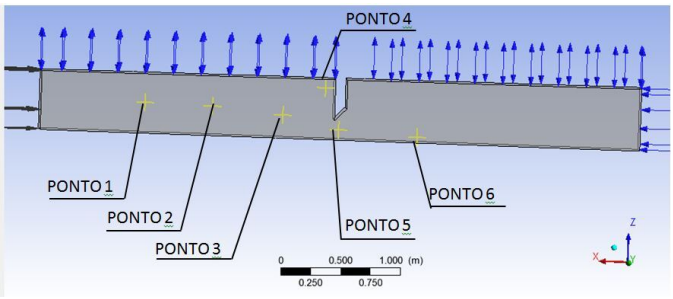

Fig. 5 Distribution of the six points analyzed along the channel.

The total simulation time was considered such that the fluid flows until the variable reaches stability, that is, when there are no significant changes in its values. For this study it was noticed that this value is approximately the time for the fluid to cross the entire domain three times. Another important definition for the study in the transient state is the time step adopted. This will be defined according to the convergence of the Courant number. For this, the intermediate mesh (Mesh 3) was chosen, as it is a mesh with a refinement that provides a low computational cost combined with a small divergence in the results of the more refined meshes. Thus, it was simulated, according to **Table 2**, each corresponding time step and Courant number, observing how the water velocity module in six points behaves, with x and y coordinates according to **Table 3**, along the channel, as shown in **Fig. 5**.

The arrangement of these points was chosen according to the flow's importance. In the upstream region, as it has a higher volume of water, four points were inserted to monitor the water speed module. Also, a point was inserted below the penstock and another point downstream of the penstock. Then, the variation of the water velocity modulus over time was simulated for different Courant numbers for the six points, as shown in **Fig. 6a–f**.

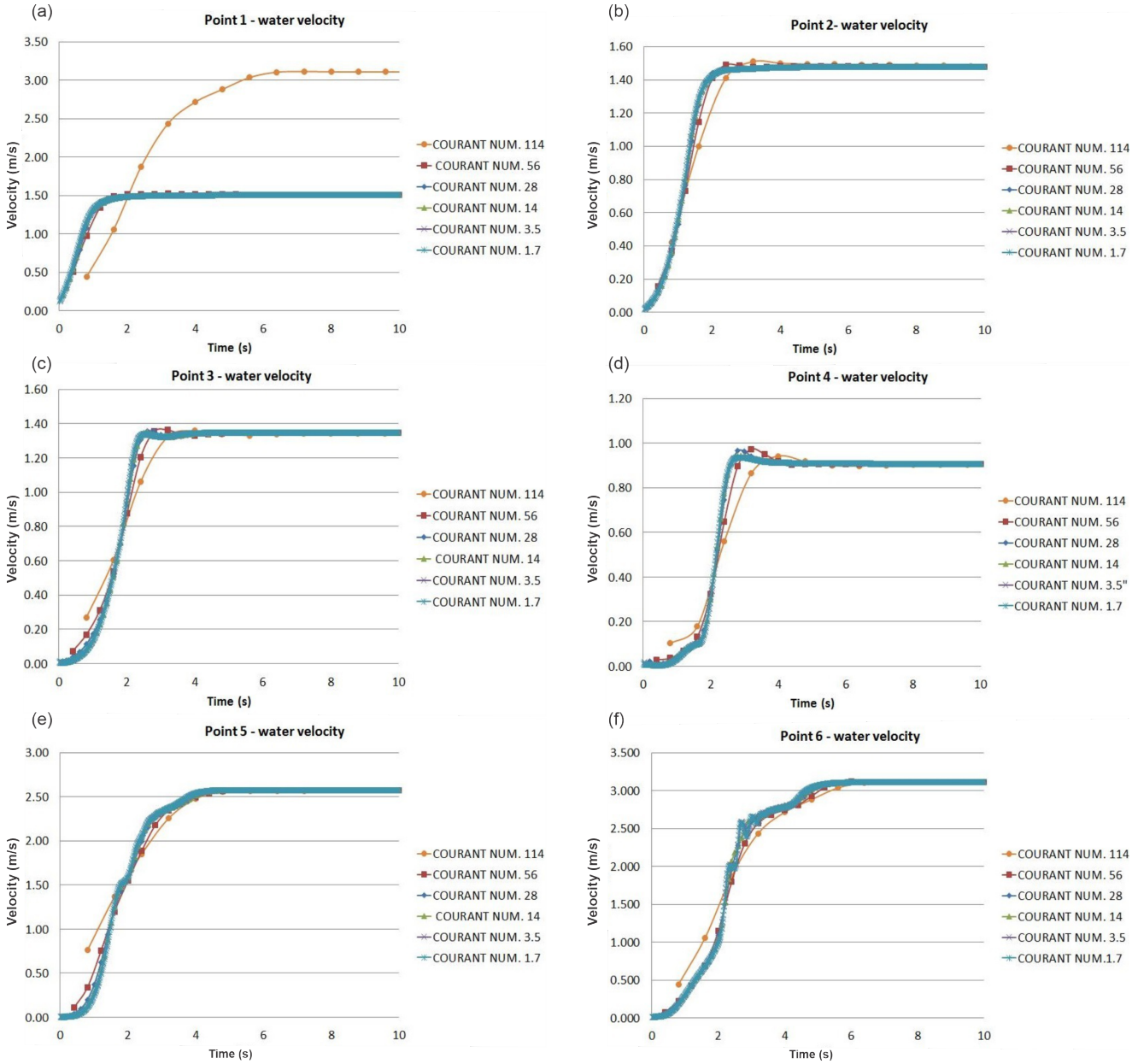

Fig. 6 Variation of the water velocity modulus over time for different Courant numbers - Point 1 (a), Point 2 (b), Point 3 (c), Point 4 (d), Point 5 (e), Point 6 (f).

Point 1 presented the greatest variation observed in relation to the velocity module referring to the several simulated Courant numbers, this is due to the fact that it is the closest point to the entrance face of the hydraulic flow. The simulation values with the Courant number equal to 114 are totally different from the others. In the remaining points, it can be observed that the simulated values with Courant numbers equal to 114 and 56 have always had the greatest oscillations in relation to the others, this is due to the fact that the time steps used for these simulations are not representative enough to capture the flow behavior. However, excluding point 1, for all other points, the speed modules were sent to the same value in the permanent state. **Table 4** with the water velocity values, at the time equal to 8.00s, in the six points studied, for the Courant numbers equal to 1.7, 3.5, 14, 28, 56 and 114. In addition, this table also shows the maximum difference between the water velocity values for the simulations with the highest Courant numbers.

Number of Iterations for each Time Step

Ansys CFX also has a standard number of iterations for each time step, this value was also checked to ensure the best number of iterations. Thus, it was simulated for the values of 2, 5, 10 (standard number of iterations per time step, suggested by the software) and 20, obtaining the water velocity value over time at the six defined points. The simulations were performed in the intermediate mesh (Mesh 3) and the stopping criterion was to obtain the stability of the values, as shown in **Fig. 7a–f.**

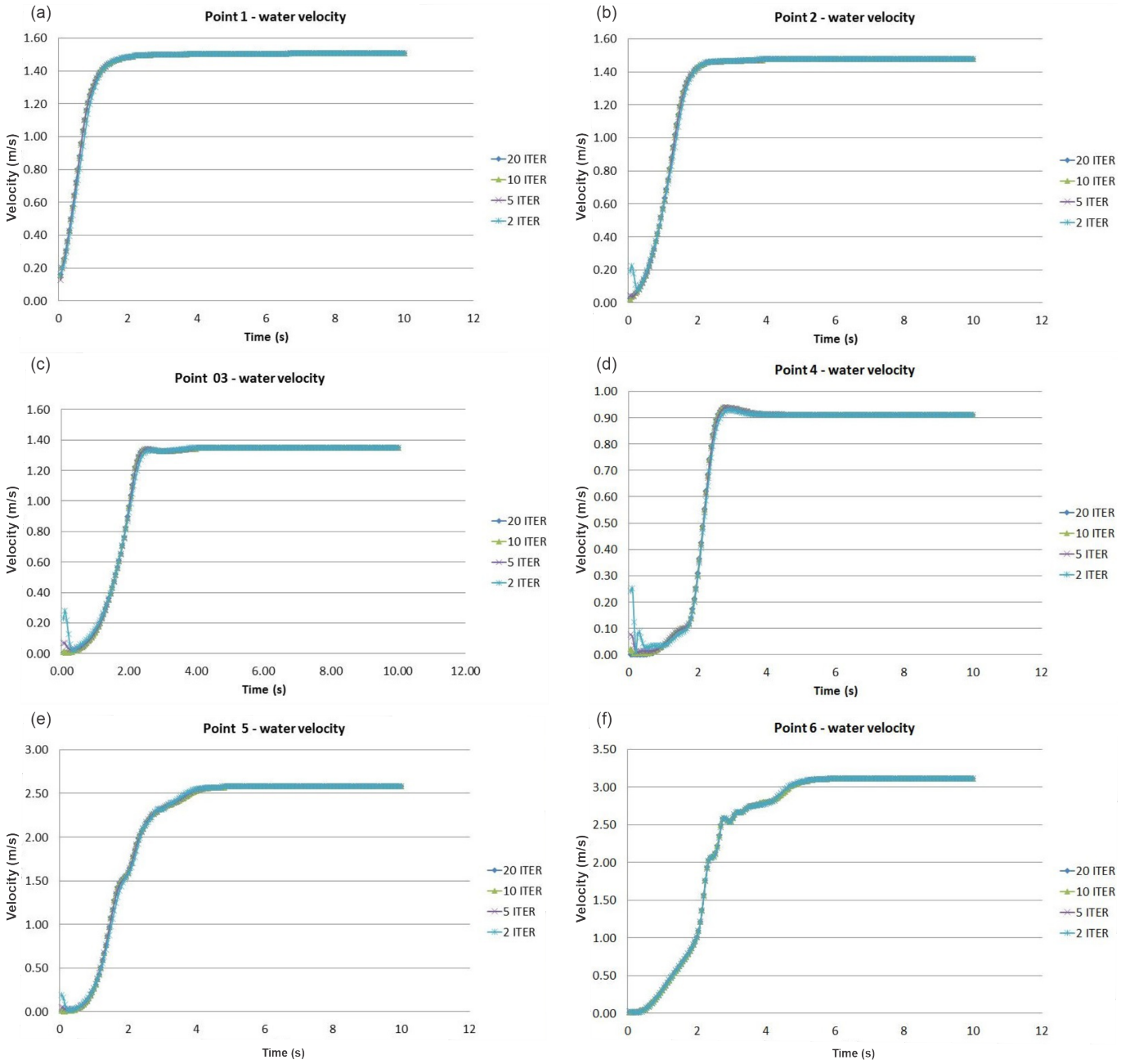

Fig. 7 Variation of the water velocity modulus over time for different numbers of iterations for each time step - Point 1 (a), Point 2 (b), Point 3 (c), Point 4 (d), Point 5 (e), Point 6 (f).

Table 4. Speed values according to the Courant number.

Courant number	Point 1	Point 2	Point 3	Point 4	Point 5	Point 6
1.7	1.506	1.478	1.347	0.908	2.577	3.112
3.5	1.506	1.478	1.347	0.908	2.577	3.112
14	1.506	1.478	1.347	0.908	2.577	3.112
28	1.506	1.478	1.347	0.908	2.577	3.112
56	1.508	1.480	1.346	0.907	2.576	3.112
114	1.521	1.486	1.344	0.902	2.572	3.112
Relative difference (%)	0.863	0.438	0.182	0.524	0.161	0.027

It is observed that there are no great variations in the water velocity modules over time, with the number of iterations changing for each time step. Carrying out in point 5 a more detailed study of the period that the permanence of the speed value is reached, according to **Fig. 8**, it is noted that there are oscillations in the order of 10^{-4} for the simulated speed values with 2 iterations in relation to the others.

Therefore, this number of iterations must be discarded. After the analysis, the number of 10 iterations was chosen for our simulation, according to the standard value suggested by the software, for each time step, aiming at the solution with the

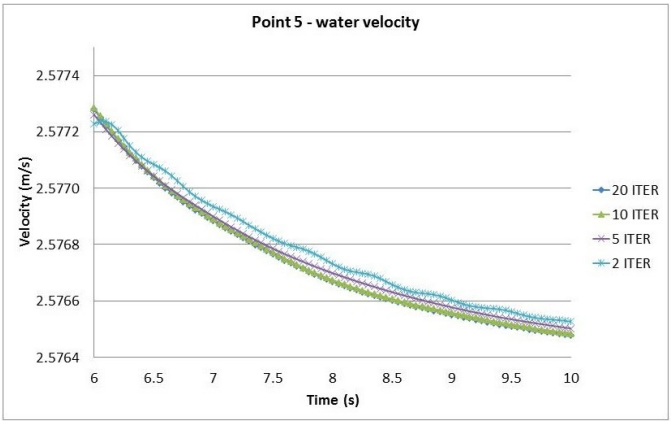

Fig. 8 Variation of the water speed module between 6.00 s to 10.00 s for different numbers of iterations - Point 5.

lowest computational cost. Next is **Table 5** with the water velocity values, at the moment equal to 6.00s, in the six points studied, for the number of iterations for each time step equal to 2, 5, 10 and 20 iterations. Furthermore, this table also shows the relative difference in percentage between the water velocity values for the simulations with the number of iterations equal to 10 and 20.

Mesh Convergence Test

In order to choose the mesh that will serve as the basis for the simulations, the mesh convergence test was performed, in this test it should be observed to what degree the mesh refinement interferes considerably in altering the final result. Then, the products of the simulations of the five meshes generated were analyzed, at the six points established and the divergence of the results was compared. The test consisted of monitoring the water velocity module throughout the process, being monitored until the value remains constant. The obtained speeds are compared and the divergences between the results are verified, according to **Fig. 9a–f**. When comparing the results of the water velocity modules after the values remain, for the five meshes, at all points, it is found that the greatest relative difference between mesh 5 and mesh 4 is 3.64% at the point 5, this shows that mesh 4 is able to represent computational modeling with the lowest cost.

Table 6 contains the water velocity values, at the moment equal to 6.00s, in the six points studied, for the five meshes. Furthermore, this table also shows a relative difference between the water velocity values for simulations with mesh 4 and 5.

Table 5. Water speed values (m / s) according to the number of iterations for each time step. Relative difference between water velocities, corresponding to the number of iterations equal to 10 and 20. Instant equal to 6.00 s.

Number of iterations for each time step	Point 1	Point 2	Point 3	Point 4	Point 5	Point 6
2	1.505	1.478	1.347	0.909	2.577	3.108
5	1.505	1.477	1.347	0.909	2.577	3.109
10	1.505	1.477	1.347	0.909	2.577	3.109
20	1.505	1.477	1.347	0.909	2.577	3.109
Relative difference (%)	0.000	0.000	0.000	0.000	0.000	0.001

Table 6. Water speed values (m/s) at the six points for the five simulated meshes. Relative difference between the speed of the water, of meshes 4 and 5. Instant equal to 6.00 s.

Mesh	Point 1	Point 2	Point 3	Point 4	Point 5	Point 6
1	1.526	1.503	1,370	0.909	2.228	2.793
2	1.518	1.481	1.347	0.862	2.545	2.886
3	1.503	1.471	1.347	0.910	2.576	3.062
4	1.502	1.480	1.343	0.951	2.594	3.111
5	1.502	1.479	1.329	0.955	2.691	3.093
Relative difference (%)	0.045	0.048	1.055	0.423	3.769	0.569

Verification

Every simulation was carried out with the channel completely full in order to study how the recirculation zone behaves, which is a strong turbulence zone as described by Rajaratnam & Humphries (1982), in this case. According to Cassan & Belaud (2012), this zone occurs at -1 <x / b <0, which goes from the base of the penstock to the bottom of the channel. Profiles of the module of the longitudinal component of the water velocity (u) were plotted at points x = -1.00m, x = -0.50m, x = -0.10 m and x = -0.02 m, as shown in **Fig. 10**, in the middle of the channel section.

These profiles are similar to those obtained by Rajaratnam & Humphries (1982) (**Fig. 11**), identifying the sudden variation of the component of the longitudinal velocity to the channel. The speed profile becomes uniform as it moves upstream from the gate. However, when approaching the wall the profile becomes more distorted, due to the deceleration of the flow caused by the bus.

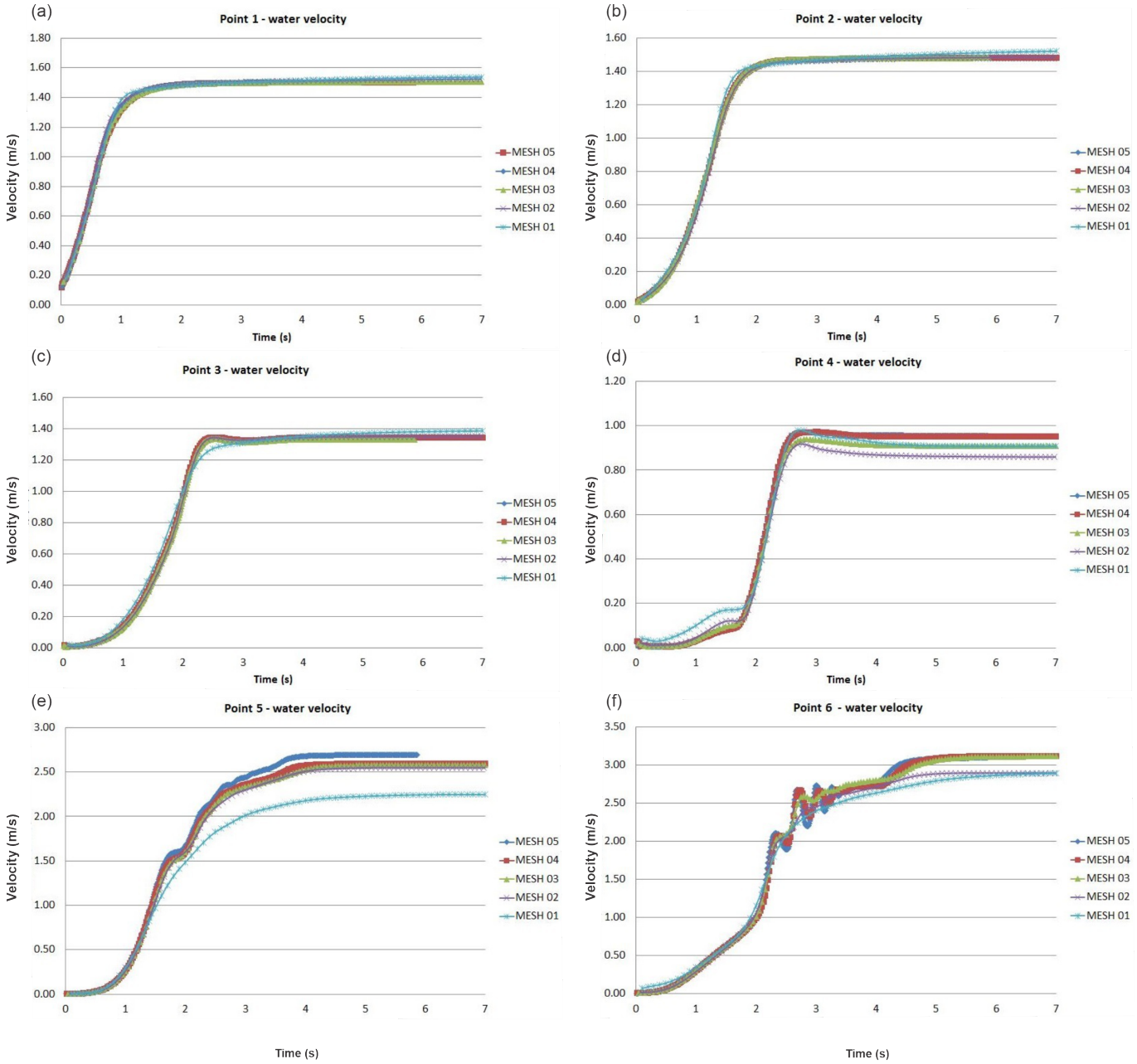

Fig. 9 Variation of the water velocity modulus over time for all modeled meshes - Point 1 (a), Point 2 (b), Point 3 (c), Point 4 (d), Point 5 (e), Point 6 (f).

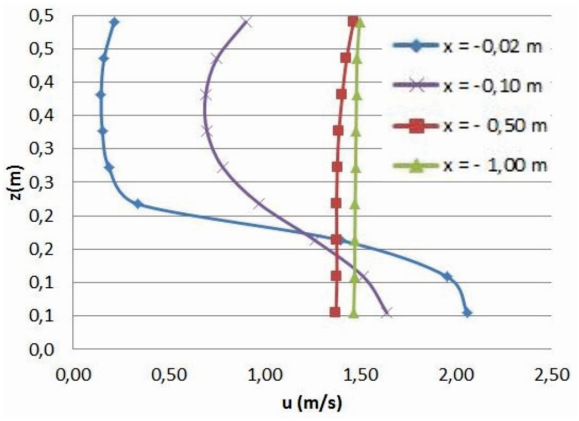

Fig. 10 Profiles of the component of the longitudinal water velocity to the channel for b = 15 cm. Source - Rajaratnam & Humphries (1982).

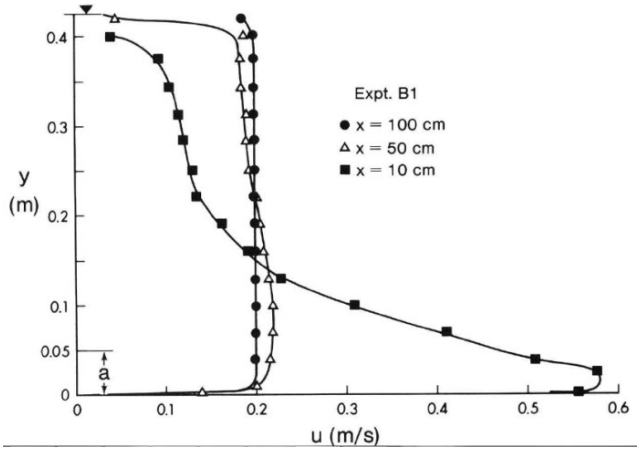

Fig. 11 Profiles of the longitudinal water velocity component to the channel, obtained experimentally.

The profile of the free surface of the flow below the floodgate modeled numerically in the present work was also compared **(Fig. 13**), with the experimental results of the workflow of Akoz *et al*. (2009) (**Fig. 12**), for the mesh that has the same contraction coefficient of the simulated model, Cc equal to 0.73 and the standard k-ε was simulated with the same turbulence model.

From the comparison of the free surface profile of the hydraulic flow below the gate, obtained experimentally by Akoz *et al.* (2009), with the numerical simulation in this work, it can be observed that there are no major divergences in the shape of the flow surface. In addition, there are no imperfections such as hydraulic adhesions at the base of the penstock. According to Porto (2006), the flow undergoes a vertical contraction until reaching a value of the liquid sheet $y_2 = Ccb$, where b is the value of the gate opening, at a distance of x = 0.00m of approximately 1.3b. When analyzing the generated numerical model, the maximum contraction is 1.333b from the same point (**Fig. 14**).

The equivalence of the modeled results with those obtained in previous works with experimental measurements confirms that the model used adequately represents the studied flow phenomenon.

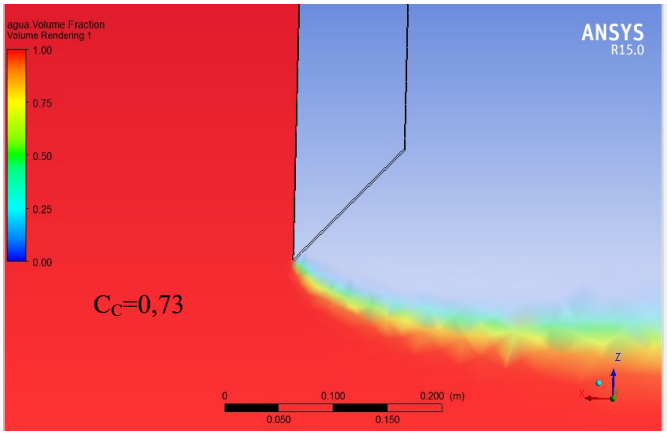

Fig. 13 Computational free surface profile in the region below the gate.

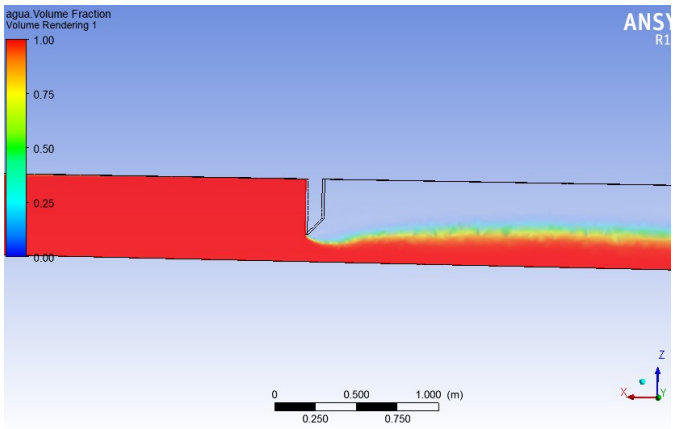

Fig. 14 Computational free surface profile downstream of the gate.

RESULTS

To analyze the behavior of the recirculation zone in fully filled channels, the profile of the velocity component perpendicular to the base of the channel (w) normalized with the initial flow velocity (V_0), in relation to the vertical position (z) normalized with the gate opening (W), in position x = 2.00 cm (**Fig. 15**). The profile reached null values close to the bottom of the cane and just below the average height of the channel section, indicating that the recirculation zone is, in the case of full channels, displaced from the surface. These results are similar to those obtained by researchers Cassan & Belaud (2012) (**Fig. 16**). This phenomenon can be observed in the representation of the flow lines, as shown in **Fig. 17**. It can also be inferred that above the recirculation zone, in full channels, there is an increase in the flow speed, so the recirculation zone becomes a zone of separation of the flow. flow where part is directed out of the channel and another part flows under the gate.

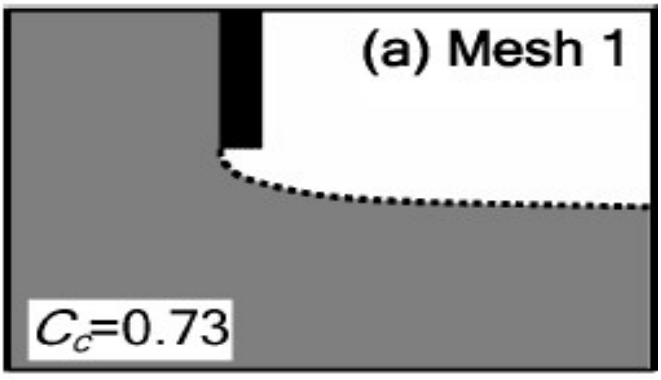

Fig. 12 Computational and experimental free surface profile in the region below the penstock, using the standard k-ε turbulence model for mesh 1. The dashed line represents the experimental free surface profiles. Source: Akoz *et al.* (2009).

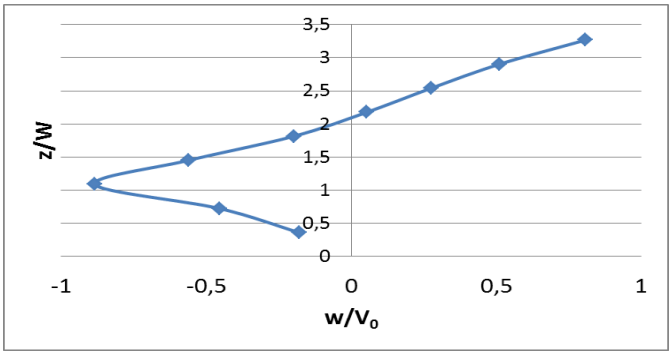

Fig. 15 Profile of the velocity component perpendicular to the base of the channel, for x = 2 cm.
Source: Cassan & Belaud (2012)

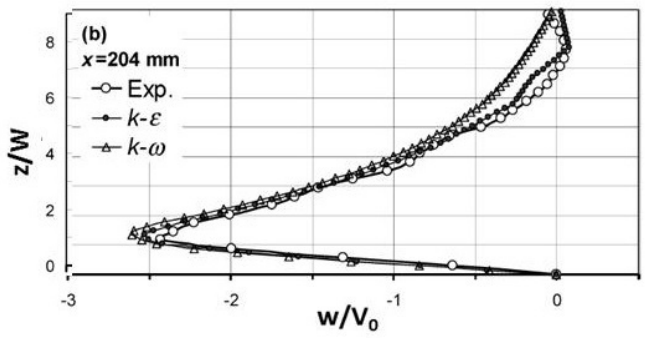

Fig. 16 Profile of the velocity component perpendicular to the base of the channel.

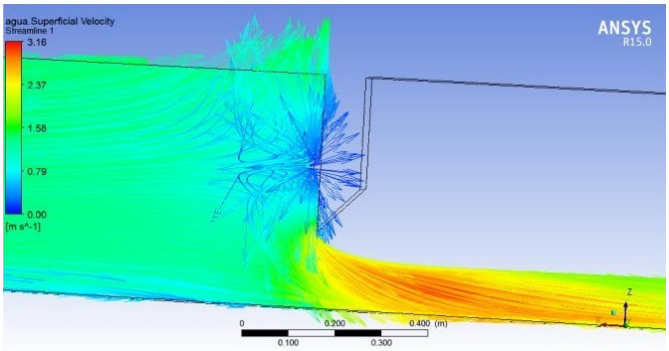

Fig. 17 Flow lines of the water speed module.

In **Fig. 18**, we can see the relative pressure diagram on the channel wall in Pascal, note that the highest values are at the bottom of the channel, due to the height of the water column, reaching a value of 5215.39 Pascal, and in the region upstream of the penstock, where it perceived the formation of the flow separation zone, this region has a relative pressure of 4593.19 Pascal, this fact indicates a region of greater pressure in the penstock structure in situations of extreme floods and maximum filling of the channel. The difference in stresses along the gate causes mechanical efforts that must be considered by structural designers when mechanically dimensioning these parts.

Another point of emphasis is the representation of the flow colliding on the upstream face of the penstock, as shown in **Fig. 19**, which represents the vector diagram of the water velocity module. The directions of the vectors, in the region of the flow separation zone, have the opposite direction to the flow. At the top, the flow is parallel to the gate, indicating the flow out of the domain. In addition, the more superficial layers of the hydraulic flow are directed out of the domain.

Figure 20 indicates the variation of water fraction in the simulated domain. The representation of the aeration layer of the hydraulic flow downstream of the gate can be seen, where there is an intense mixture between the two components of the two-phase model, air and water. This layer tends to increase with the development of the flow, aerating the flow downstream of the hydraulic device.

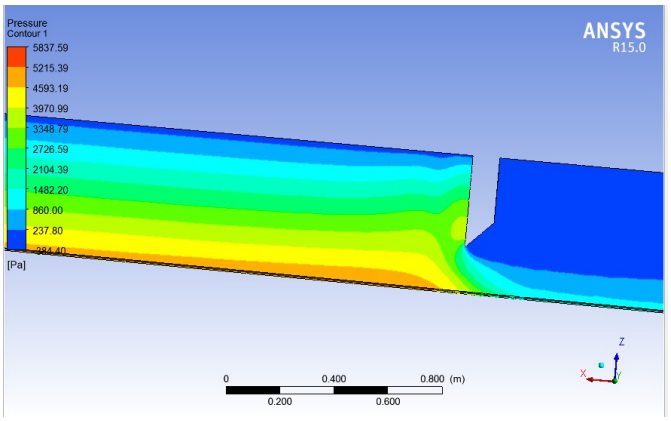

Fig. 18 Pressure diagram at 7.00s.

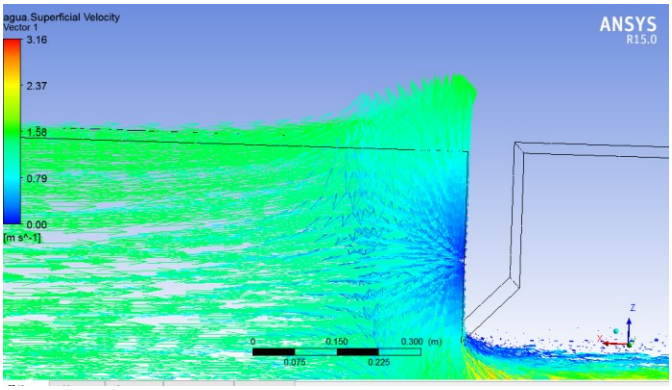

Fig. 19 Vector diagram of water speed at the moment equal to 7.00s.

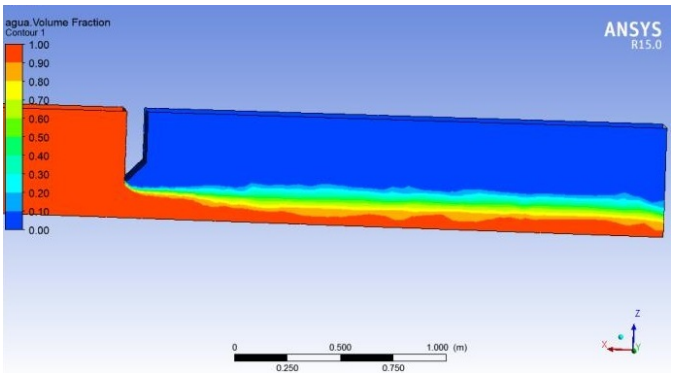

Fig. 20 Variation of water and air phases, red represents water and blue represents air, the remaining colors represent variation in concentration between phases.

CONCLUSIONS

This work uses a numerical model to characterize the flow in a channel subject to its maximum capacity with a partially open hydraulic gate, in order to simulate a defect in the operation of the structure that prevents its complete opening.The study demonstrated that the steady state (permanent) should only be used for initial estimates of the flow parameters in channels with maximum flood. The number of iterations for each time step had a less relevant impact for the model studied, because the method of solving equations is robust.

The variation in the number of mesh elements caused greater changes in the hydraulic flow values. In future applications it is necessary to test meshes with different amounts of elements until arriving at a mesh that, when refined, no longer changes the results.

The model identified a flow recirculation zone near the floodgate and that the flow velocity close to it is zero. This zone is also a flow separation region. Still, there is an increase in the pressure values in the floodgate region, close to this zone.

Numerical tools using computational fluid dynamics proved to be sufficiently advanced to help in the analysis of the flow under the floodgate subject to extreme situations of floods and mechanical failures that hinder the opening of the structure.

The CFD simulation proved to be very promising and indicated for the analysis of multiphase flows in channels with hydraulic gates. It is of great importance, because its three-dimensional, biphasic and free-surface models obtain results very close to reality, helping to choose the appropriate geometry and reducing project costs.

REFERENCES

Ahmed, U., Apsley,D., Stallard, T., Stansby,P. & Afgan, I. (2020) Turbulent length scales and budgets of Reynolds stress-transport for open-channel flows; friction Reynolds numbers (Reτ) = 150, 400 and 1020, *Journal of Hydraulic Research* **59**(1), 36-50, doi: 10.1080/00221686.2020.1729265.

Akoz, M. S., Kirkgoz, M. S., Oner, A. A. (2009) Experimental and numerical modeling of a sluice gate flow. *Journal of Hydraulic Research* **47** (2), 167-176.

Cassan, L. & Belaud, G. (2012) Experimental and numerical investigation of flow under sluice gates. *Journal of Hydraulic Div*., *ASCE* **138**(4), 367-373.

Celik, I. B., Ghia, U., Roache, P. J., Freitas, C. J., Coleman, H. & Raad, P. E. (2008) Procedure for estimation and reporting of uncertainty due to discretization in CFD applications. *Journal of Fluids Engineering* **130**(1), 1–4.

Çengel, Y. A. & Cimbala, J.M. (2007) *Mecânica dos fluidos fundamentos e aplicações*. Mc Graw Hill, AMGH.

Ciocan, T., Susan-Resiga, F. R., & Muntean, S. (2016) Modelling and optimization of the velocity profiles at the draft tube inlet of a Francis turbine within an operating range, *Journal of Hydraulic Research*, **54**(1), 74-89.

Faure, J.-B., Buil, N. & Gay, B. (2004) 3-D modeling of unsteady free-surface flow in open channel. *Journal of Hydraulic Research* **42**(3), 263-272.

Ferdos, F. & Dargahi, B. (2016) A study of turbulent flow in largescale porous media at high Reynolds numbers. Part I: numerical validation, *Journal of Hydraulic Research* **54**(6), 663-677, doi: 10.1080/00221686.2016.1211184.

Ferdos, F. & Dargahi, B. (2016) A study of turbulent flow in largescale porous media at high Reynolds numbers. Part II: flow physics, Journal of Hydraulic Research 54(6), 678-691, doi: 10.1080/00221686.2016.1211185.

Hardy, R. J., Lane, S. N., Lawless, M.R., Best, J.L., Elliott, L. & Ingham, D. B. (2005) Development and testing of a numerical code for treatment of complex river channel topography in three-dimensional CFD models with structured grids, *Journal of Hydraulic Research* **43**(5), 468-480.

Jesudhas, V., Roussinova, V., Balachandar, R. & Barron, R. (2016) Submerged hydraulic jump study using DES. *Journal of Hydraulic Engineering* **143**(3).

Jesudhas, V., Balachandar, R. & Bolisetti, T. (2019): Numerical study of a symmetric submerged spatial hydraulic jump, *Journal of Hydraulic Research* 58(2), 335-349, doi: 10.1080/00221686.2019.1581668.

Koutrouveli, T. I., Dimas, A. A., Fourniotis, N. T. & Demetracopoulos, A. C. (2018) Groyne spacing role on the effective control of wall shear stress in open-channel flow, *Journal of Hydraulic Research* **57**(2), 167-182, doi: 10.1080/00221686.2018.1478895.

Launder, B. E. & Spalding, D. B. (1974) The numerical computation of turbulent flows. *Computer Methods in Applied Mechanics and Engineering* **3**(2), 269-289.

Li, Y., Wang, X., Xuan, G. & Liang, D. (2019) Effect of parameters of pool geometry on flow characteristics in low slope vertical slot fishways, *Journal of Hydraulic Research* **58**(3), 395-407 doi: 10.1080/00221686.2019.1581666.

Li, Z., Bi, H., Karney, B., Wang, Z. & Yao. Z. (2017) Threedimensional transient simulation of a prototype pump-turbine during normal turbine shutdown, *Journal of Hydraulic Research* **55**(4), 520-537.

Lin, C.H., Yen, J.F. & Tsai, C.T. (2002) Influence of sluice gate contraction coefficient on distinguishing condition. *Journal Irrigation and Drainage Engineering*, *ASCE* **128**(4), 249-252.

Lira, V.M.P. (2014) Numerical modeling of a 90° open-channel confluence using Openfoam CFD. Dissertação. MSc Thesis, Universidade Federal de Minas Gerais, Belo Horizonte, Brazil.

Lu, Y., Su, X. & Li, J. (2018) A topology-alterative two-phase flow solver and its validation for a dynamic hydraulic discharge process, *Journal of Hydraulic Research* **57**(5), 607-622, doi: 10.1080/00221686.2018.1489902

Maranzoni, A. & Tomirotti, M. (2020) 3D CFD analysis of the performance of oblique and composite side weirs in converging channels, *Journal of Hydraulic Research*, doi:10.1080/00221686.2020.1818304.

Momplot, A., Kouyi, G.L., Mignot, E., Rivière, N. & Krajewski, J.L.B. (2016) Typology of the flow structures in dividing open channel flows. *Journal of Hydraulic Research* **55**(1), 63-71.

Momplot, A., Kouyi, G. L., Mignot, E., Rivière, N. & Bertrand-Krajewski, J. (2016) Typology of the flow structures in dividing open channel flows, *Journal of Hydraulic Research* **55**(1), 63-71, doi: 10.1080/00221686.2016.1212409.

Rajaratnam, N. & Humphries, J. A. (1982) Free flow upstream of vertical sluice gates. *Journal of Hydraulic Research* **20**(5), 427-437.

Porto, R. M. (2006) *Hidráulica Básica*. *EESC USP*.

Sanagiotto, D. G., Rossi, J. B. & Bravo, J. M. (2019) Applications of computational fluid dynamics in the the design and rehabilitation of nonstandard vertical slot fishways. *Water* **11**(2), 199.

Sinha, J., Samir, K. Das., Patel, P.L. & Samtani, B.K. (2014) Development of two-layered model for compound open-channel flow, *ISH Journal of Hydraulic Engineering* **20**(3), 250-262.

Talebpour, M. & Liu, X. (2018) Numerical investigation on the suitability of a fourth-order nonlinear k-ω model for secondary current of second type in openchannels, *Journal of Hydraulic Research* **57**(1), 1-12, doi: 10.1080/00221686.2018.1444676.

Taylor, Z. H., Carlston, J. S. & Venayagamoorthy, S. K. (2015) Hydraulic design of baffles in disinfection contact tanks, *Journal of Hydraulic Research* **57**(1), 1-12, doi: 10.1080/00221686.2015.1040086.

Teng, P. & Yang, J. (2016) CFD modeling of two-phase flow of a spillway chute aerator of large width. *Journal of Applied Water Engineering and Research* **4**(2), 163-177.

Versteeg, H. K. & Malalasekera, W. (2007) *An introduction to computational fluid dynamics - the finite volume method.* Second. Ed, Essex: Pearson Prentice Hall.

Yang, B., Deng, J., Yuan, W. & Wang, Z. (2019) Investigation on continuous pressure wave in a periodic transient flow using a three-dimensional CFD model, *Journal of Hydraulic Research*, doi: 10.1080/00221686.2018.1555553.

Zhang, B., Wu, B., Li, S. & Shi, Y. (2020) Large eddy simulation of sediment transport in high flow intensity by discrete particle method, *Journal of Hydraulic Research*, DOI: 10.1080/00221686.2020.1818306.